Cui *et al. Energy Mater* 2023;3:300017
DOI: 10.20517/energymater.2022.83

Energy Materials

Article

Open Access

Check for updates

Polyurethane/$Li_{10}GeP_2S_{12}$ composite electrolyte with high ions transfer number and ions capture for all-solid-state lithium batteries

Peng Cui, Chun Sun, Wei Wei*

College of Electronic and Optical Engineering, Nanjing University of Posts & Telecommunications, Nanjing 210023, Jiangsu, China.

***Correspondence to:** Prof. Wei Wei, College of Electronic and Optical Engineering, Nanjing University of Posts & Telecommunications, 9 Wenyuan Road, Nanjing 210023, Jiangsu, China. E-mail: weiwei@njupt.edu.cn

How to cite this article: Cui P, Sun C, Wei W. Polyurethane/$Li_{10}GeP_2S_{12}$ composite electrolyte with high ions transfer number and ions capture for all-solid-state lithium batteries. *Energy Mater* 2023;3:300017. https://dx.doi.org/10.20517/energymater.2022.83

Received: 25 Nov 2022 **First Decision:** 9 Feb 2023 **Revised:** 28 Feb 2023 **Accepted:** 15 Mar 2023 **Published:** 7 Apr 2023

Academic Editors: Yuping Wu, Meicheng Li **Copy Editor:** Fangling Lan **Production Editor:** Fangling Lan

Abstract

Polymer/ceramic composite electrolytes have recently received a lot of attention because they combine the advantages of high ionic conductivity of inorganic ceramics and the inherent elasticity of polymer constituents. Nonetheless, the interaction between the ceramic particles and the polar functional groups on the polymer molecules would affect the ion transport rate, which is an important factor to consider when developing a polymer/ceramic composite electrolyte. We present a composite elastic electrolyte based on polyurethane (PU) with high ionic conductivity of 10^{-3} S/cm and excellent mechanical properties (stress-strain) of 4.5 MPa by incorporating ceramic particles into the ion conduction chains on PU. This method improves the interaction between PU/LGPS and Li^+ ions and the conduction of Li^+ ions at the bi-phase interface, yielding a high Li^+ transfer number of 0.56. After 2,000 cycles, the capacity retention rates of the batteries assembled by [LFP|(PU-LGPS)/Li^+|Li] are 95.7% (0.2 C) and 87.8% (5 C), respectively. The Li symmetric battery test demonstrates the PU/LGPS composite electrolyte's high stability over 50 days. The current study presents a novel approach to developing high-performance ceramic/polymer composite electrolytes.

Keywords: Polymer/ceramic composite electrolytes, ions transfer number

INTRODUCTION

All-solid-state Li-ion batteries (ASSLBs) have been regarded as an alternative to traditional liquid Li-ion batteries (LLIBs) for their higher energy density, better safety, and flame retardancy[1]. The core component of ASSLBs is the solid-state electrolyte (SSE), which is linked to the overall performance of the battery[2]. Among all types of SSEs, $Li_{10}GeP_2S_{12}$(LGPS)[3] exhibits a high ionic conductivity (10^{-2} S/cm), which is comparable to liquid electrolytes. However, the main drawbacks of inorganic solid electrolytes are their poor flexibility and high interfacial impedance between electrolyte and electrodes[4,5]. It has been discovered that the presence of high interfacial impedance reduces the capacity retention and operating efficiency at high C-rates and long cycles, lowering the battery's overall performance[6,7].

Additionally, solid polymer electrolyte (SPE) has many advantages, such as flexibility and good film formation ability[8], which can compensate for the disadvantage of inorganic solid electrolytes. Therefore, preparing polymer/ceramic composite electrolytes is an effective strategy for overcoming the drawbacks of inorganic ceramic electrolytes. At present, physical mixing with different polymer/inorganic ratios is a simple and easy method to screen the optimal composite electrolyte systems[9-11]. Therefore, researchers paid little attention to the impact of the interaction of polymer and inorganic ceramic molecules on Li^+ ions. In addition, as for SPE, the ionic conductivity, as well as the ionic transfer number, are also key factors for choosing the polymer substrate [most polymers have low ionic conductivity(10^{-5}~10^{-6} S/cm)[9] and the ionic transfer number(< 0.5)[12].

In our previous work[2], we prepared a PU-based SPE with excellent mechanical properties and high ionic conductivity at room temperature (2×10^{-3} S/cm). Since the PU-based SPE has a unique soft and hard segment structure, Li^+ ions primarily transport in polyether polyols (PPG), so the soft segment in the PU-based SPE has the ability to dissolve lithium salts[13-15] and disperse ceramic particles[16].

In this study, a composite electrolyte [(PU-LGPS)/Li^+, PLL] was created by modifying the soft segment functional groups in a PU-based electrolyte and incorporating LGPS particles (1~5 μm) into the polymer systems. In this study, Fourier transform infrared (FTIR) spectroscopy, Raman spectra, and X-ray photoelectron spectroscopy (XPS) were used to characterize the structure and properties of PLL. Meanwhile, we used the electrochemical impedance spectroscopy (EIS) test and assembled the battery to evaluate the specific charge/discharge capacity and electric cycle stability at room temperature. Furthermore, using first-principles simulation, we investigated the mechanism of the composite system that improves Li^+ transport.

RESULTS AND DISCUSSION

Figure 1 depicts the PLL preparation process. Supplementary Material Section 1 shows all materials and preparation details. PPG (20 g, 0.03 mol) first reacts with $LiOH{\cdot}H_2O$ (5 g, 0.1 mol) to change the functional groups from "-OH" to "-OLi". The mixture was then supplemented with LiTFSI (1 g, 3 mmol) and Al_2O_3 (0.05 g, 0.4 mmol) and stirred for 2 h until fully dissolved. Following that, LGPS (5 g, 8 mmol) particles were added, and the solution was evenly stirred to form a homogeneous solution. Finally, the 7.5 mmol MDI was added to form PLL. We can disperse the LGPS primarily in soft segment chains using this method, and the interaction of Al_2O_3 with functional groups has been described in our previous work[2].

Infrared and Raman spectra were used to characterize the PU and the effects of different LGPS addition ratios on functional groups and chemical bonds. Infrared spectra characterized the chemical component and internal bonding behavior of PU, and the change in peak position after the addition of LGPS (a detailed analysis of the analyzed infrared spectra) is shown in Supplementary Material Figure 1A[17-19].

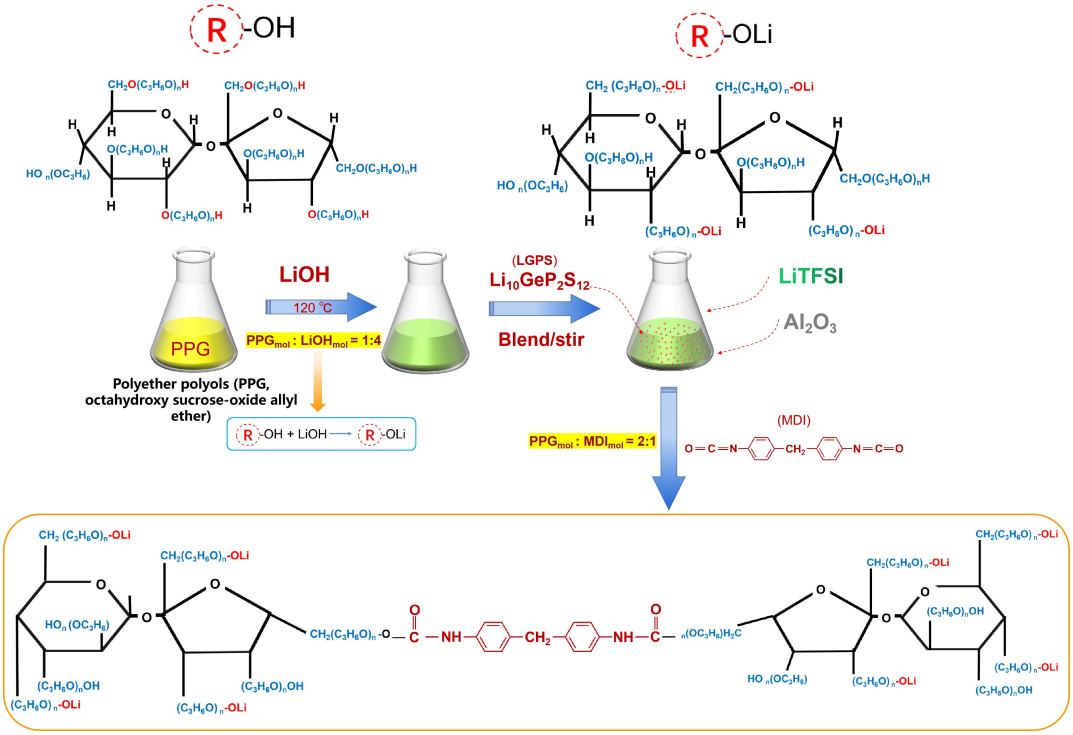

Figure 1. The preparation process of PLL [(PU-LGPS)/Li^+]

Supplementary Figure 1B depicts the Raman spectra of PU and PU + LGPS. The Raman characteristic peaks at 275 cm^{-1}, 409 cm^{-1}, and 556 cm^{-1}[20-21] can be ascribed to the deformation vibration peak, stretching vibration peak, and asymmetric vibration absorption peak of PS_4^{3-} and $P_2S_7^{4-}$, respectively. The stretching vibration of LiS_4^{3-} causes the absorption peak at 341 cm^{-1}. Furthermore, the stretching vibration peak of the "P-S-P" bond can cause the absorption peak at 512 cm^{-1}[22]. The obtained results show that the composite material PLL has good chemical compatibility [Figure 2].

We used XPS characterization to further investigate the bonding behavior of the composite electrolyte, and the results are shown in Table 1.

Through the XPS analysis of the PLL, it can be known that the PLL's internal state is stable.

In addition, the physical properties of PLL are also critical, which are associated with electrolyte thermal stability and mechanical properties. Furthermore, the surface morphology of PLL is shown to efficiently identify element distribution in PLL and PLL affinity for various fillers.

First, we examined the XRD patterns of PU and LGPS, respectively. The sample LGPS peak location [Supplementary Figure 2] is consistent with the simulation XRD patterns[30]. The figure shows that the prepared PU material has a broad peak at 2θ near 19.5° and 46.0°, indicating that the prepared PU material has a certain degree of crystallinity[31].

Figure 3A presents that the glass transition temperature (T_g) value was approximately -51 °C, indicating that the electrolyte has good flexibility at ambient temperatures. Figure 3B displays the stress-strain curve for PLL. It demonstrates that PLL has a stress strength of 4.5 MPa and an elongation-at-break level of 220.1%.

Table 1. Details of XPS analysis for PLL

Elements	Main morphology	Binding energy (eV)	Peak position	Proportion(%)
1-S 2p	-S-	161.65	2p3/2	25.83
		162.95	2p1/2	
	O=S=O[23]	168.66	2p3/2	
		169.79	2p1/2	
1-P 2p	P[24]	133.12	2p3/2	
		134.22	2p1/2	
1-Li 1s	Li-S[25] Li-O[26]	55.69		
1-Ge 3d	Ge[27]	25.78	Ge 3d5/2	70.48
		26.55	Ge 3d3/2	
	GeO	29.87		16.17
	GeO_2	33.86		13.34
1-C1s	C-C/C-H	284.8		41.37
	C-O[28]	286.34		55.79
	O-C=O[29]	289.01		2.83

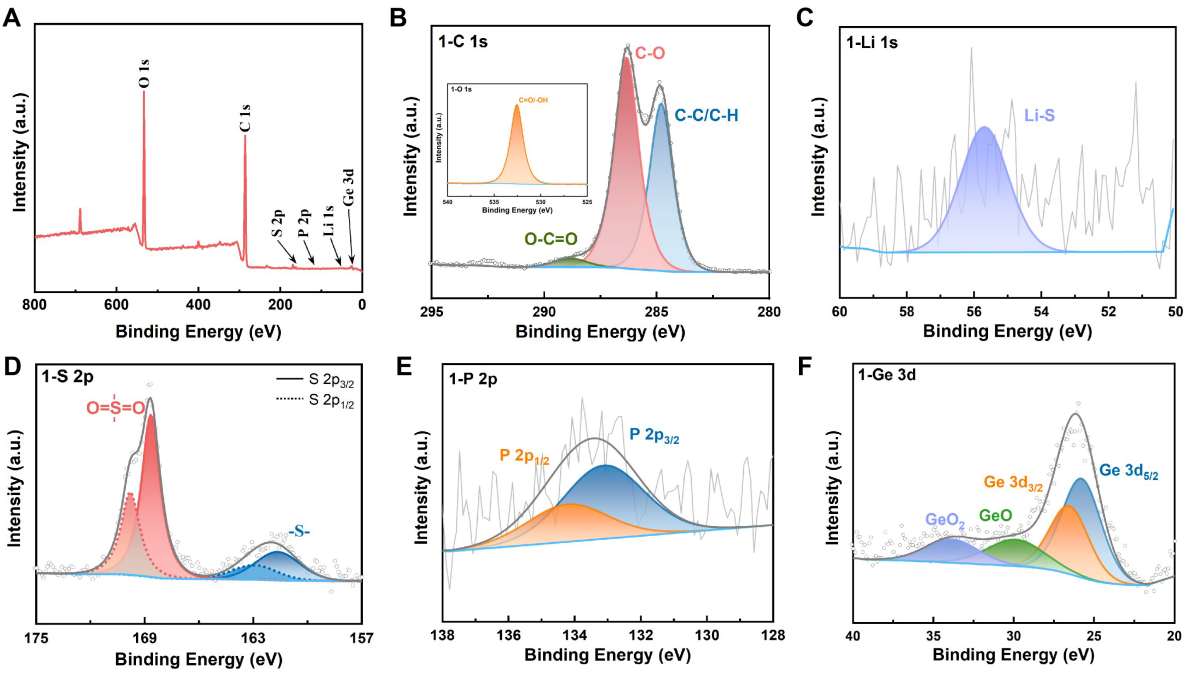

Figure 2. XPS spectra of electrolyte PLL. (A) full spectrum diagram; (B) C_{1S}, illustrations: O_{1S}; (C) Li_{1S}; (D) S_{2P}; (E) P_{2P}; (F) Ge_{3d}.

These characterizations show that PLL has good stress strength characteristics, with higher stress-strain properties compared to other reported SPEs[32]. Supplementary Figure 3 clearly shows an SEM image for surface morphology and element mapping for electrolyte PLL. Besides, the electrolyte surface is smooth and evenly distributed, and the elements found in reactant LGPS are present in this electrolyte system. Al_2O_3 nanoparticles and LiTFSI within the polymer system are evenly distributed in this system, indicating that these added fillers are compatible with the system[2].

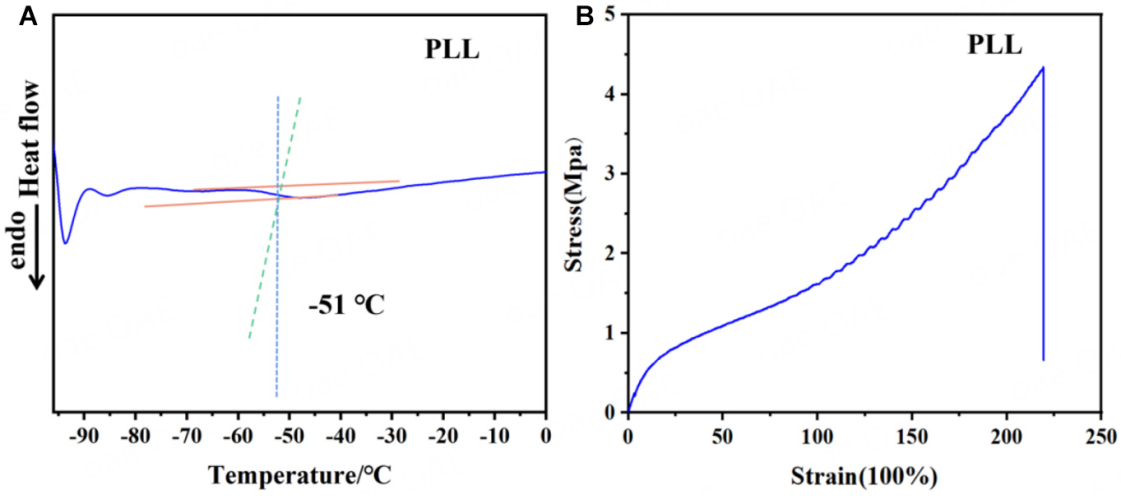

Figure 3. (A) DSC curve of the PLL; (B) the stress-strain curve of the as-prepared PLL.

Ionic conductivity is an important electrolyte parameter. Table 2 details the ionic conductivity changes caused by various (LGPS/PU = x)/Li^+ ratios.

Although the ionic conductivity of PLL continues to rise with the increase of LGPS, for electrolytes, in addition to the ionic conductivity, the stress-strain performance is considered a vital index to evaluate the Li dendrite inhibition ability of the electrolyte.

Figure 4A shows the Arrhenius plots for the ionic conductivities of different proportions of (LGPS/PUx)/Li^+. Through the slope of these curves, the relationship between the ionic conductivity and temperature of several groups of samples was established. The linear relation between temperature and conductivity demonstrates that PLL electrolytes obey the ion transport mechanism originating from the polymer chain vibration mechanism. Figure 4B explains the metric for screening the optimal electrolyte systems. Three samples with proportions of 30%, 40%, and 50% were selected. Since the conductivity of the sample with a 60% proportion is not much higher than that of the sample with a 50% proportion, and its mechanical property is also lower than that of the three samples (30%, 40%, and 50%), we did not consider the sample with 60%. The activation energies of the three different proportions of (LGPS/PU)/Li^+ were 149.3 kJ/mol (30%), 64.6 kJ/mol (40%), and 34.7 kJ/mol (50%), respectively [Supplementary Figure 4]. The activation energy calculation details are shown in Supplementary Material Section 1. Figure 4B demonstrates the relationship between ionic conductivity and stress. The sample with an LGPS ratio of 40% has superior mechanical properties than that of the sample with 50%. As a result of extensive analysis, the optimal proportion of PLL is 40%.

Figure 4C displays the AC impedance of a PLL at different temperatures. As the temperature rises from 25 °C to 80 °C, the conductivity rises from 3.1×10^{-3} to 6.1×10^{-3} S/cm. The ionic conductivity can be identified through polymer chain movement based on Li^+ coordination and interaction based on the elevation of ionic conductivity as temperature increases[33]. As shown in Figure 4D, the linearity of Arrhenius plots for ionic conductivity as a function of temperature suggests that polymer electrolyte conductivity follows Arrhenius law[34].

Table 2. Ionic conductivity of PLL with LGPS adding an amount

Samples	$(LGPS/PU_x)/Li^+$, X = 10%~80%	R (Ω)	Conductivity (S cm^{-1})
1	10%	21.2	1.2×10^{-3}
2	20%	10.6	2.4×10^{-3}
3	30%	9.2	2.9×10^{-3}
4	40%	8.3	3.1×10^{-3}
5	50%	6.5	3.9×10^{-3}
6	60%	5.7	4.5×10^{-3}
7	70%	5.2	4.9×10^{-3}
8	80%	4.7	5.4×10^{-3}

Sample thickness: 200 um; electrolyte area: $S = \pi r^2$ (r = 0.05 cm): π/4.

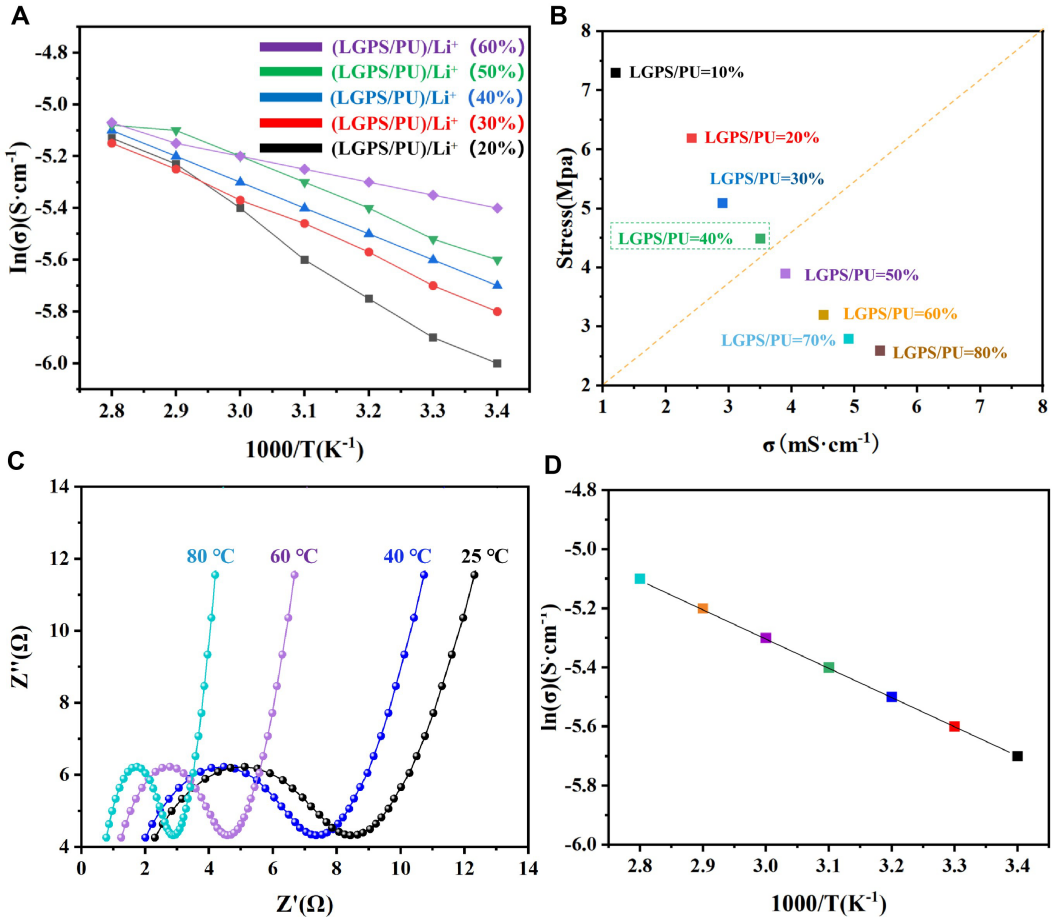

Figure 4. (A) Arrhenius plots for the ionic conductivities of different proportions of $(LGPS/PUx)/Li^+$; (B) Relationship between ionic conductivity and stress, PLL at different temperatures; (C) AC impedance; and (D) Arrhenius plots for the ionic conductivities (40%).

This study determined the ionic transfer number of the composite to further demonstrate Li^+ transfer kinetics. Figure 5 clearly shows the potentiostatic polarization curve and the variation of the impedance spectra before and after the polarization of the PLL composite Figure 5A. Furthermore, the value of T_{Li} is 0.56, and the ionic transference number calculation details are shown in Supplementary Material Section 2.

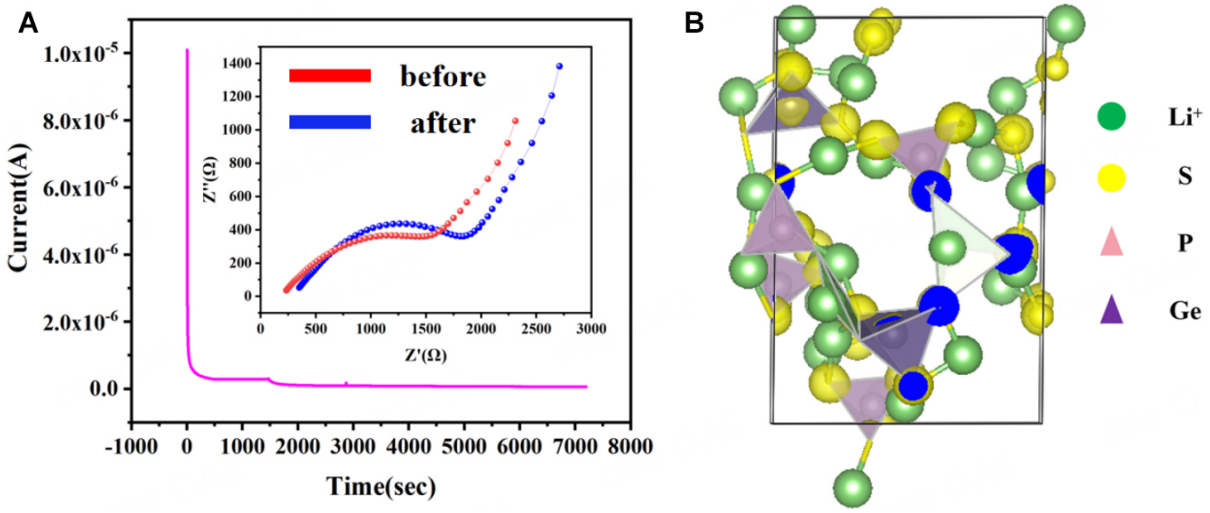

Figure 5. (A) Potentiostatic polarization curve of a symmetric lithium battery (Li|PLL|Li), the illustrations are the impedance comparison of a symmetric lithium battery(Li|PLL|Li) before and after polarization; (B) First-principles theory simulation analyzing the charge distribution in the LGPS crystal.

To investigate the charge distribution in the LGPS crystal, we used first-principles theory simulation[35-37]. Figure 5B depicts the charge being primarily concentrated around "S" atoms, demonstrating the ease with which electron exchange can occur. Based on previous research, we demonstrated that "O" atoms can act as Li^+ trapping sites due to dense negative charge distributions surrounding "O" atoms. These findings suggest that Li^+ deintercalated from the LGPS lattice can be absorbed by "O" atoms on PU. Furthermore, the functional group modification process can reduce the coupling impact of "O" atoms on Li^+, resulting in a moderate capture behavior. The absorption energy of the "-OLi" group towards Li^+ is shown to be 0.55 eV in comparison to that of the "-OH" group (1.01 eV)[2], indicating that the "-OLi" group can both capture and easily give out the Li^+ from LGPS crystal. Therefore, the "-OLi" group can function as a Li^+ transfer medium, and the "S" sites in the LGPS crystal, in conjunction with the "O" site on the PU molecule, can function as an interfacial ion transfer channel, contributing to the high ionic conductivity.

The LFP|PLL|Li battery was built to investigate the use of an electrolyte for battery device performance. Figure 6A depicts specific LFP|PLL|Li battery capacities at different cycle C-rates. At 0.2 C, the capacity was 167.7 mAh/g, which was very close to the theoretical specific capacity of LFP cathode materials (170 mAh/g). It can show that the PLL electrolyte is effective at transporting ions and contacting solid-state LFP|PLL|Li battery electrodes. Furthermore, our assembled battery has high stability in the charging/discharging platform under varying C-rates with no polarization, indicating that our prepared electrolyte significantly improves battery stability while improving electrolyte-electrode contact, reducing the phenomenon of battery polarization. Figure 6B depicts the battery charging/discharging process at various C-rates. When the cycling rate is changed from 0.2 C to 5 C and then back to 0.2 C, the battery capacity reaches 99%, indicating that the internal rate of the battery is stable. Figure 6C depicts a schematic plot of the battery during the bulb-lighting process.

Figure 6D depicts the long-cycle performance of the batteries based on varying C-rates. After 2,000 cycles, the battery retention rate can still be 95.7% at 0.2 C, 91% at 3 C, and 87.8% at 5C, indicating the assembled batteries' excellent performance stability.

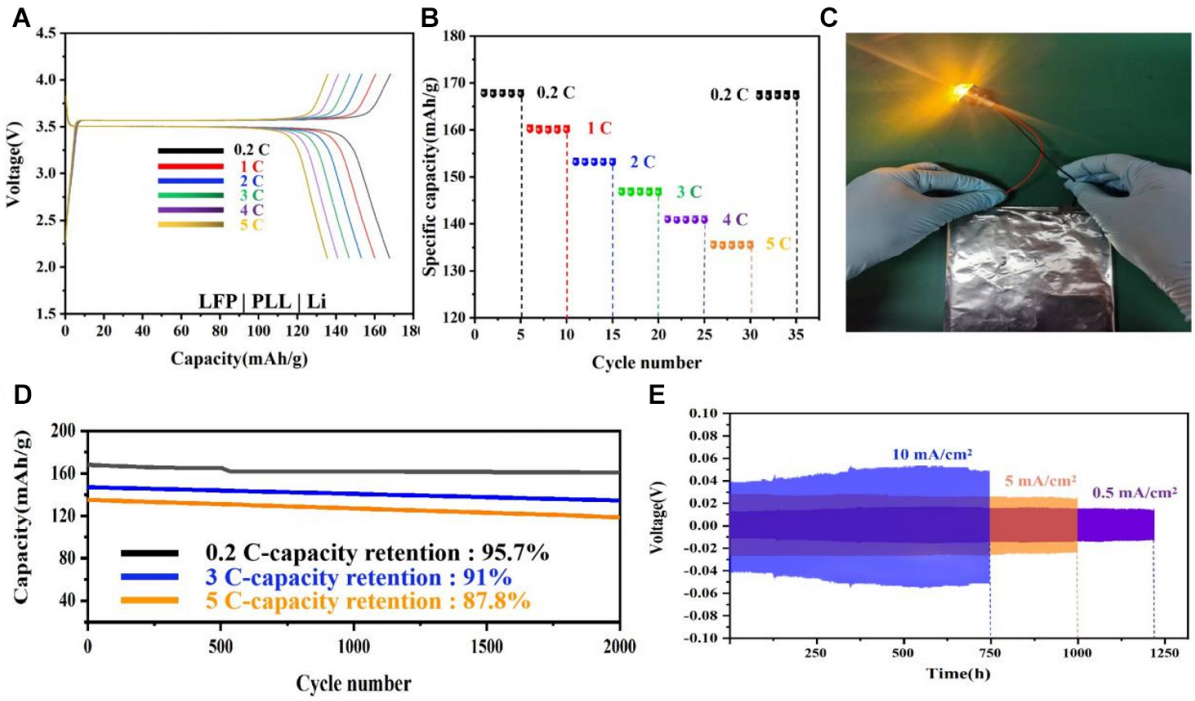

Figure 6. (A) LFP|PLL|Li, the first charge/discharge curves for 0.2 C, 1 C, 2 C, 3 C,4 C, and 5 C at ambient temperatures; (B) Capacity with various C-rates; (C) Battery luminescence picture (LFP|PLL|graphite); (D) Long-cycling properties offered based on varying C-rates; (E) Voltage-time curves of the symmetric lithium battery (Li|PLL|Li) at the current density of 0.5 mA/cm^2 and 5 mA/cm^2, as well as 10 mA/cm^2.

The voltage profiles of the symmetric Li|PLL|Li cells at 0.5 mA/cm^2, 5 mA/cm^2, and 10 mA/cm^2 are shown in Figure 6E. The cells maintained stable voltage profiles for 1,250 h at 0.5 mA/cm^2. When the current is increased tenfold (5 mA/cm^2), the voltage fluctuation increases from 0.01 V to 0.03 V. Despite the increased fluctuation range, the circulation remained stable within 1,000 h, indicating no obvious polarization phenomenon appeared. With the current density increased to 10 mA/cm^2, more than 700 h of stable circulation and hysteresis can be obtained, indicating the good stability of Li|PLL|Li batteries. Through the investigation of the electrolyte PLL and the overall performance analysis of the assembled batteries, which are superior to previous reports[38-40] [Table 3]. We assembled an NCM|PLL|Li battery to verify that PLL has a universal adaptive electrode. The results [Supplementary Figure 5A] demonstrate that the PLL we developed can be adapted to the NCM electrode. Furthermore, 40 cycles were performed at 5 C to compare the two groups of batteries (NCM|PLL|Li battery and LFP|PLL|Li battery), and both groups of batteries had stable cycles, demonstrating the excellent performance of the PLL prepared by us [Supplementary Figure 5B].

As shown in Table 4, when the current density of the PLL is increased from 0.5 mA/cm^2 to 10 mA/cm^2, the voltage increases by 0.04 V. However, in some other relevant works[41,42,44,45], the current density was still less than 0.5 mA/cm^2. Despite the fact that Deng's work[43] increased the current density to 4.5 mA/cm^2, the voltage fluctuation value was 0.5 V. In contrast, there is no obvious polarization phenomenon in the PLL electrolyte. This result shows that the PLL electrolyte has a high intrinsic ionic conductivity. PU is an elastic electrolyte that can form a good contact interface with the electrode, promoting interfacial ion transport.

Table 3. Comparison of the ionic conductivity and ions transfer number of the electrolytes, and cycle performance of assembled solid-state batteries regarding their capacity and rate and retention

Electrolyte	Ionic conductivity (S/cm)	Ions transfer number (t_{Li}^+, 25 °C)	Batteries performances LFP as cathode
This work: PLL, [(PU-LGPS)/Li^+]	3.1×10^{-3} (25 °C) 6.1×10^{-3} (80 °C)	0.56	SC[a] : 167.7 mAh/g at 0.2 C CR[b]: at 2000 cycles 95.7% at 0.2 C; 91.0% at 3 C; 87.8% at 5 C
PEO/Li^+-LGPS[38]	1.18×10^{-5} (25 °C) 1.21×10^{-3} (80 °C)	0.26	SC: 158 mAh/g at 0.1 C 148 mAh/g at 0.2 C 138 mAh/g at 0.5 C 99 mAh/g at 1 C CR: at 50 cycles, 92.5% at 0.1 C, (60 °C)
PEO/Li^+-PEG-LGPS[39]	9.83×10^{-4} (25 °C) 1.72×10^{-3} (60 °C)	0.68	SC: 168 mAh/g at 0.05 C 166 mAh/g at 0.1 C 158 mAh/g at 0.5 C CR: at 150 cycles , 91% at 0.5 C
PEO/Li^+-1%LGPS-10%SN[40]	9.1×10^{-5} (25 °C)	0.2	SC: 160.6 mAh/g at 0.1 C CR: at 60 cycles, 94.7% at 0.1 C at 100 cycles, 87.65% at 0.5

[a]: SC, specific capacity; [b]: CR, capacity retention.

Table 4. Comparison of voltage variations of different polymer solid electrolytes at different current densities

Electrolyte	Ionic conductivity	Current (mA/cm^2)/polarization (V)
This work: PLL	3.1×10^{-3} (25 °C) 6.1×10^{-3} (80 °C)	0.5/ -0.01~0.01 5/-0.03~0.03 10/-0.05~0.05
SLICPs[41]	1×10^{-4} (80 °C)	0.1/-0.01~0.01
PCPU[42]	1.12×10^{-4} (80 °C)	0.2/-0.2~0.2
CPE-PHCE[43]	-	0.3/-0.15~0.15 4.5/-0.6~0.6
PVAE[44]	-	0.3/-0.25~0.25
PEO/CuF_2[45]	2×10^{-4} (30 °C)	0.1/-0.075~0.075

CONCLUSIONS

In conclusion, a new solid composite electrolyte PLL [(PU-LGPS)/Li^+] was developed. LGPS particles are dispersed in soft segment structure (PPG) on PU, and functional groups "-OH" and ionic bonds "-OLi" interactions on PPG and LGPS are used to promote Li^+ transport. The PLL has a high Li^+ transfer number of 0.56 as well as increased ionic conductivity [3.1×10^{-3} S/cm (25 °C), 6.1×10^{-3} S/cm (80 °C). Moreover, we used the first-principles theory to confirm the enhancement mechanism of ion transport in the dual system. The batteries that we have assembled perform admirably. The specific discharge capacity at 0.2 C was nearly 167.7 mAh/g, which approaches the theoretical specific capacity of LFP materials (170 mAh/g), resulting in excellent capacity retention (95.7%) after 2,000 cycles at 0.2 C, as well as retention of 91% and 87.8% after 2,000 cycles at 3 C and 5 C, respectively. This research provides a solid theoretical foundation and experimental demonstration for preparing composite polymer electrolytes, which improve battery efficiency.

DECLARATIONS

Authors' contributions

Were responsible for conceiving the idea: Cui P, Sun C, Wei W

Carried out the material synthesis, cell fabrication, and battery testing; Explored the material characterization data; Accounted for writing the manuscript: Cui P, Sun C
Conducted the electrochemical measurements and cathode characterization: Cui P
Accounted for performing the first-principles simulation and also offered the analysis: Sun C
Was responsible for editing the manuscript: Wei W
All the authors have discussed the findings, read the manuscript, and also approved its content.

Availability of data and materials

All materials and preparation details are shown in the Supplementary Material, Supplementary Material Section 1.

Financial support and sponsorship

The present study was financially funded by the National Natural Science Foundation of China [grant numbers: 62075100] as well as the Jiangsu Postgraduate Research Innovation Program [grant numbers: KYCX20_0701].

Conflicts of interest

All authors declared that there are no conflicts of interest.

Ethical approval and consent to participate

Not applicable.

Consent for publication

Not applicable.

REFERENCES

1. Goodenough J, Kim Y. Challenges for rechargeable batteries. *J Power Sources* 2011;196:6688-94. DOI
2. Cui P, Zhang Q, Sun C, et al. High ion conductivity based on a polyurethane composite solid electrolyte for all-solid-state lithium batteries. *RSC Adv* 2022;12:3828-37. DOI PubMed PMC
3. Kamaya N, Homma K, Yamakawa Y, et al. A lithium superionic conductor. *Nat Mater* 2011;10:682-6. DOI
4. Goodenough JB, Kim Y. Challenges for rechargeable Li batteries. *Chem Mater* 2010;22:587-603. DOI
5. Chan CK, Yang T, Mark Weller J. Nanostructured garnet-type $Li_7La_3Zr_2O_{12}$: synthesis, properties, and opportunities as electrolytes for Li-ion batteries. *Electrochim Acta* 2017;253:268-80. DOI
6. Shen Y, Zhang Y, Han S, Wang J, Peng Z, Chen L. Unlocking the energy capabilities of lithium metal electrode with solid-state electrolytes. *Joule* 2018;2:1674-89. DOI
7. Cheng X, Zhao C, Yao Y, Liu H, Zhang Q. Recent advances in energy chemistry between solid-state electrolyte and safe lithium-metal anodes. *Chem* 2019;5:74-96. DOI
8. Zhou Q, Ma J, Dong S, Li X, Cui G. Intermolecular chemistry in solid polymer electrolytes for high-energy-density lithium batteries. *Adv Mater* 2019;31:e1902029. DOI PubMed
9. Chen R, Qu W, Guo X, Li L, Wu F. The pursuit of solid-state electrolytes for lithium batteries: from comprehensive insight to emerging horizons. *Mater Horiz* 2016;3:487-516. DOI
10. Li Z, Huang HM, Zhu JK, et al. Ionic conduction in composite polymer electrolytes: case of PEO:Ga-LLZO composites. *ACS Appl Mater Interfaces* 2019;11:784-91. DOI PubMed
11. Ju L, Wang Y, Pan Y, Feng L. Preparation and conductivity characteristic of PEO-$Li_{1.3}Al_{0.3}Ti_{1.7}(PO_4)_3$ composite polymer electrolytes. *J Mater Sci Eng* 2014;6:867-70. DOI
12. Xin S, You Y, Wang S, Gao H, Yin Y, Guo Y. Solid-state lithium metal batteries promoted by nanotechnology: progress and prospects. *ACS Energy Lett* 2017;2:1385-94. DOI
13. Bao J, Tao C, Yu R, Gao M, Huang Y, Chen C. Solid polymer electrolyte based on waterborne polyurethane for all-solid-state lithium ion batteries. *J Appl Polym Sci* 2017;134:45554. DOI

14. Wen TC, Du YL, Digar M. Compositional effect on the morphology and ionic conductivity of thermoplastic polyurethane based electrolytes. *Eur Polym J* 2002;38:1039-48. DOI
15. Bar N, Basak P. Quasi-solid semi-interpenetrating polymer networks as electrolytes: part II. Assessing the modes of ion-ion and ion-polymer interactions employing mid-fourier transform infrared vibrational spectroscopy. *J Phys Chem C* 2014;118:10640-50. DOI
16. Cui P, Sun C, Dai H, Wei W. Polyurethane-P_2S_5 composite-based solid-state electrolyte assists low polarization and high stability all-solid-state lithium-ion batteries. *RSC Adv* 2022;12:27881-8. DOI PubMed PMC
17. Badri KBH, Sien WC, Shahrom M, Hao LC, Baderuliksan NY, Norzali NR. FTIR spectroscopy analysis of the prepolymerization of palm-based polyurethane. *Solid State Sci Technol* 2010;18:1-8. Available from: https://scholar.google.com/citations?view_op=view_citation&hl=ja&user=pNmzBRcAAAAJ&citation_for_view=pNmzBRcAAAAJ:u-x6o8ySG0sC [Last accessed on 6 April 2023]
18. Hatchett DW, Kodippili G, Kinyanjui JM, Benincasa F, Sapochak L. FTIR analysis of thermally processed PU foam. *Polym Degrad Stab* 2005;87:555-61. DOI
19. Tang Q, Gao K. Structure analysis of polyether-based thermoplastic polyurethane elastomers by FTIR, ^{1}H NMR and ^{13}C NMR. *Int J Polym Anal Charact* 2017;22:569-74. DOI
20. Sourisseau C, Cavagnat R, Fouassier M, Brec R, Elder SH. Infrared, Raman, resonance Raman spectra and lattice dynamics calculations of the solid potassium (I) nickel (II) thiophosphate compound, $KNiPS_4$. *Chem Phys* 1995;195:351-69. DOI
21. Sang L, Haasch RT, Gewirth AA, Nuzzo RG. Evolution at the solid electrolyte/gold electrode interface during lithium deposition and stripping. *Chem Mater* 2017;29:3029-37. DOI
22. Sharma P, Jha PK, Diwan P, Pandey O. Impact of CuS on the crystallization kinetics of Na_2S-P_2S_5 glasses. *J Non Cryst Solids* 2017;477:31-41. DOI
23. Zhu J, Jian T, Wu Y, et al. A highly stable aqueous Zn/VS_2 battery based on an intercalation reaction. *Appl Surf Sci* 2021;544:148882. DOI
24. Guo W, Zhang W, Si Y, Wang D, Fu Y, Manthiram A. Artificial dual solid-electrolyte interfaces based on in situ organothiol transformation in lithium sulfur battery. *Nat Commun* 2021;12:3031. DOI PubMed PMC
25. Balamurugan S, Naresh N, Prakash I, Satyanarayana N. Capacity fading mechanism of Li_2O loaded $NiFe_2O_4$/SiO_2 aerogel anode for lithium-ion battery: ex-situ XPS analysis. *Appl Surf Sci* 2021;535:147677. DOI
26. Wang Z, Li X, Guo W, Fu Y. Anion intercalation of VS_4 triggers atomic sulfur transfer to organic disulfide in rechargeable lithium battery. *Adv Funct Mater* 2021;31:2009875. DOI
27. Tallapally V, Nakagawara TA, Demchenko DO, Özgür Ü, Arachchige IU. $Ge_{1-x}Sn_x$ alloy quantum dots with composition-tunable energy gaps and near-infrared photoluminescence. *Nanoscale* 2018;10:20296-305. DOI PubMed
28. Zhang S, Liu C, Wang H, et al. A covalent P-C bond stabilizes red phosphorus in an engineered carbon host for high-performance lithium-ion battery anodes. *ACS Nano* 2021;15:3365-75. DOI PubMed
29. Fan L, Ma R, Zhang Q, Jia X, Lu B. Graphite anode for a potassium-ion battery with unprecedented performance. *Angew Chem Int Ed* 2019;131:10610-5. DOI PubMed
30. Ma J, Quhe R, Zhang Z, et al. Two-dimensional materials as a stabilized interphase for the solid-state electrolyte $Li_{10}GeP_2S_{12}$ in lithium metal batteries. *J Mater Chem A* 2021;9:4810-21. DOI
31. Trovati G, Sanches EA, Neto SC, Mascarenhas YP, Chierice GO. Characterization of polyurethane resins by FTIR, TGA, and XRD. *J Appl Polym Sci* 2010;115:263-8. DOI
32. Chen B, Xu Q, Huang Z, Zhao Y, Chen S, Xu X. One-pot preparation of new copolymer electrolytes with tunable network structure for all-solid-state lithium battery. *J Power Sources* 2016;331:322-31. DOI
33. Baik J, Kim D, Shim J, Lee JH, Choi Y, Lee J. Solid polymer electrolytes containing poly(ethylene glycol) and renewable cardanol moieties for all-solid-state rechargeable lithium batteries. *Polymer* 2016;99:704-12. DOI
34. Bandyopadhyay S, Marzke R, Singh R, Newman N. Electrical conductivities and Li ion concentration-dependent diffusivities, in polyurethane polymers doped with lithium trifluoromethanesulfonimide (LiTFSI) or lithium perchlorate ($LiClO_4$). *Solid State Ion* 2010;181:1727-31. DOI
35. Perdew JP, Burke K, Ernzerhof M. Generalized gradient approximation made simple. *Phys Rev Lett* 1996;77:3865-8. DOI PubMed
36. Blöchl PE. Projector augmented-wave method. *Phys Rev B Condens Matter* 1994;50:17953-79. DOI PubMed
37. Hafner J. Ab-initio simulations of materials using VASP: density-functional theory and beyond. *J Comput Chem* 2008;29:2044-78. DOI PubMed
38. Zhao Y, Wu C, Peng G, et al. A new solid polymer electrolyte incorporating $Li_{10}GeP_2S_{12}$ into a polyethylene oxide matrix for all-solid-state lithium batteries. *J Power Sources* 2016;301:47-53. DOI
39. Pan K, Zhang L, Qian W, et al. A flexible ceramic/polymer hybrid solid electrolyte for solid-state lithium metal batteries. *Adv Mater* 2020;32:e2000399. DOI PubMed
40. Chen B, Huang Z, Chen X, et al. A new composite solid electrolyte PEO/$Li_{10}GeP_2S_{12}$/SN for all-solid-state lithium battery. *Electrochim Acta* 2016;210:905-14. DOI
41. Fei Y, Liu S, Long Y, et al. New single lithium ion conducting polymer electrolyte derived from delocalized tetrazolate bonding to polyurethane. *Electrochim Acta* 2019;299:902-13. DOI
42. Bao J, Shi G, Tao C, et al. Polycarbonate-based polyurethane as a polymer electrolyte matrix for all-solid-state lithium batteries. *J Power Sources* 2018;389:84-92. DOI

43. Deng T, Cao L, He X, et al. In situ formation of polymer-inorganic solid-electrolyte interphase for stable polymeric solid-state lithium-metal batteries. *Chem* 2021;7:3052-68. DOI
44. Tian Z, Hou L, Feng D, Jiao Y, Wu P. Modulating the coordination environment of lithium bonds for high performance polymer electrolyte batteries. *ACS Nano* 2023;17:3786-96. DOI PubMed
45. Wei Y, Liu T, Zhou W, et al. Enabling all-solid-state Li metal batteries operated at 30 °C by molecular regulation of polymer electrolyte. *Adv Energy Mater* 2023;13:2203547. DOI